RSC Advances

PAPER

View Article Online
View Journal | View Issue

Cite this: *RSC Adv.*, 2024, **14**, 3900

Methane hydrate efficient formation in a 3D-rGO/SDBS composite†

Meijiao Wang,[a] Shaojiu Yan,*[ab] Nan Wang,[b] Wen Ge[c] and Wei Zhang[a]

The optimization of storage space and material composition can significantly improve the generation rate and storage capacity of methane hydrate, which is important for the industrial application of solidified natural gas (SNG) technology. In our report, the effects of the presence of SDBS (sodium dodecylbenzene sulfonate), GO (graphene oxide), 3D-rGO (3D-reduced graphene oxide) and 3D-rGO/SDBS (3D-reduced graphene oxide/sodium dodecylbenzene sulfonate) on the methane hydrate generation process are investigated. The results show that the heterogeneous effect on the solid-phase surface of 3D-rGO/SDBS and its interconnected three-dimensional (3D) structure can achieve rapid nucleation. In addition, the presence of 3D-rGO/SDBS can increase the dissolution and dispersion of gas in solution and further enhance the gas–liquid mass transfer, thus realizing efficient methane storage. The maximum methane storage capacity of 188 v/v_w is obtained with 600 ppm of 3D-rGO/SDBS in water, reaching 87% of the theoretical maximum storage capacity. The addition of 3D-rGO/SDBS also significantly reduces the induction time and accelerates the formation rate of methane hydrate. This study reveals that 3D graphene materials have excellent kinetic promotion effects on methane hydrate formation, explores and enriches the hydrate-promoting mechanism, and provides essential data and theoretical basis for the research of new promoters in the field of SNG technology.

Received 12th December 2023
Accepted 15th January 2024

DOI: 10.1039/d3ra08478g

rsc.li/rsc-advances

1 Introduction

In nature, the combination of methane and water under certain temperature and pressure conditions can form crystalline compounds with cage structure where water molecules form water cages by hydrogen bonding, encasing methane molecules within them.[1] Methane hydrates have a cubic structure called structure I (sI) hydrate. The structure consists of two different types of water cages: one is 6 large cages consisting of 24 water molecules with 12 pentagonal and 2 hexagonal faces (denoted as $5^{12}6^2$), the other is 2 small cages consisting of 20 water molecules with 12 pentagonal faces (denoted as 5^{12}). The average radii of the large and small cages are 0.433 and 0.395 nm. So theoretically each cage has enough space to hold one methane molecule.[2] The discovery of natural methane hydrates inspired the transportation of methane in solidified form. First of all, the formation of methane hydrates is thermodynamically favourable ("narrow" pressure range of 3–10 MPa and mild temperatures). Secondly, they have superior theoretical gas storage capacities. If all water cages were filled with methane, approximately 180 volumes (STP) of methane would be released per volume of hydrate decomposition.[3] The resulting concept of solidified natural gas (SNG) technology has received a lot of attention in recent years. In addition, compared to current mature natural gas transportation technologies such as compressed natural gas (CNG) and liquefied natural gas (LNG), which require the use of higher pressures (25 MPa and 25 °C) or lower temperatures (−162 °C and 0.1 MPa) to process the gas, the SNG technology is a safer, more economical, and more environmentally friendly alternative.

However, the formation of artificial methane hydrates in the laboratory exhibits unfavourable kinetic constraints due to (1) the low solubility of methane in water, (2) the limited contact interface between methane and water that inhibits diffusion of methane in water to the critical concentration required to initiate nucleation, and (3) the limitation of mass transfer due to the formation of a hydrate film from the aggregation of hydrate crystals at the gas–liquid interface.[4] As a result, methane hydrate formation in the pure water system (CH_4 + H_2O) exhibits low nucleation kinetics and slow growth rates, which make it difficult to generate large quantities in reasonable time scales, and the actual gas storage capacity is lower than the theoretical value. These circumstances limit the commercial development of SNG technology. By introducing solid surface to form non-homogeneous nucleation centres, the energy barrier for crystal nucleation in liquid-phase can be

[a]*Key Laboratory of Geological Survey and Evaluation of Ministry of Education, China University of Geosciences, Wuhan 430074, China. E-mail: shaojiuyan@126.com*
[b]*Research Centre of Graphene Applications, AECC Beijing Institute of Aeronautical Materials, Beijing 100095, China*
[c]*Faculty of Materials Science and Chemistry, China University of Geosciences, Wuhan 430078, China*

† Electronic supplementary information (ESI) available. See DOI: https://doi.org/10.1039/d3ra08478g

effectively reduced to accelerate the nucleation kinetics.[5,6] In recent years, there has been a rapid increase in research results on solid porous materials such as activated carbon,[7] natural sand,[8] porous glass,[9] silica powder,[10] hydrogels[11] and metal–organic frameworks[12] as host structures for methane hydrate formation. Porous materials have stable 3D space, large specific surface area and variable mineral composition, which largely increase the effective interface between the gas and liquid phases and contribute to the rapid formation of methane hydrates. The ultra-high specific surface area and excellent thermal conductivity properties of graphene materials make them of great interest in the field of gas hydrates.[13–15] Ghozatloo *et al.*[16] researched graphene prepared by the Hummers' method for the first time in the formation process of natural gas hydrates, and the results showed that using a small amount of graphene could shorten the induction time by 61.07% and increase the gas storage capacity by 12.9% compared with the pure water system. Hosseini *et al.*[17] used 1 wt% CVD graphene nanosheets to promote the formation of natural gas hydrates, and the incorporation of graphene nanosheets reduced the induction time by 54.7% and increased the gas storage capacity by 7.6%. Liu *et al.*[18] found that the addition of graphene can induce an increase in intermediate water (IW), and IW has the potential to accelerate the nucleation of methane hydrate. Compared with sodium cholate solution, the mixed solution of graphene and sodium cholate was able to shorten the induction time and generation period of methane hydrate by 47.87% and 36.90%, respectively. In addition, utilizing the self-assembly characteristics of graphene can provide ideas for the design of novel graphene-based promoters. Graphene sheets can be constructed to form 3D graphene materials with interconnected 3D structures through non-covalent π–π interactions.[19–21] 3D graphene does not mean graphite, which is layered graphene, but a 3D interconnected porous material. 3D graphene can firstly preserve the exceptional 2D physical and chemical properties of graphene, and secondly its 3D structure enables high degree of porosity, large accessible surface area and efficient mass transport, which is important for promoting the formation of methane hydrates.[22]

On the other hand, the activity of porous materials as promoters of hydrate formation also depends on their surface properties, especially the surface functional groups.[23,24] Thus, the properties of porous materials can be further enhanced by introducing surface functional groups. McElligott *et al.*[25] introduced nitrogen-containing functional groups into graphene and prepared low- and high-nitrogen doped graphene nanoflakes (LN-GNFs and HN-GNFs), which accelerated the dissolution rate of methane in the solution of LN-GNFs by 17.54% and increased the hydrate growth rate by 77.20% as compared to that of the pure water system. Wang *et al.*[26] prepared sulfonated graphene oxide (SGO) for promoting methane hydrate formation by grafting $-SO_3^-$ groups onto graphene oxide sheets. When the concentration of SGO was 0.75 g L^{-1}, most of the hydrate was formed in about 312 min, and the storage capacity reached an optimal value of 143.9 v/v (volumes of gas/volume of water). Sodium dodecylbenzene sulfonate (SDBS) is a common surfactant that increases methane solubilization in solution through nonpolar adsorption, and its $-SO_3^-$ active group also enhances the mass transfer process from the gas phase to the aqueous phase, which collectively improves methane hydrate formation.[27] Due to the presence of benzene ring, SDBS can form π-like stacking on the surface of carbon materials, which can enhance the binding of surfactant molecules to graphene, giving the surface of 3D graphene unique characteristics.[28–30] Currently, two-dimensional (2D) graphene sheets and their composites have been attempted to promote methane hydrate formation, but studies combining the unique structure of 3D graphene and surface modification to produce synergistic effects for solidified gas efficient storage have not been reported.

In this study, 3D reduced graphene oxide/sodium dodecylbenzene sulfonate (3D-rGO/SDBS) was prepared from graphene oxide (GO) and sodium dodecylbenzene sulfonate (SDBS) by combining the chemical reduction and self-assembly method with freeze-drying technique. For comparison, 3D reduced graphene oxide (3D-rGO) was also prepared. The effects of the presence of SDBS, GO, 3D-rGO and 3D-rGO/SDBS on the formation of methane hydrates were comparatively investigated using pure water as a control group, and the mechanism of action of 3D graphene-based promoters was explored in the context of the kinetic processes of methane hydrate nucleation and growth.

2 Experimental section

2.1 Materials

GO (industrial grade) was purchased from Beijing Graphene Technology Research Institute Co., Ltd (Beijing, China). SDBS (A.R.) and L-ascorbic acid (A.R.) were purchased from Sinopharm Chemical Reagent Co., Ltd (Beijing, China). Methane gas (purity of 99.9%) was supplied by Jing Gao Gas Co., Ltd (Beijing, China). Deionized water was laboratory-made and the resistivity was 18.3 MΩ cm (298.15 K).

2.1.1 Preparation of 3D-rGO. The GO suspension was first prepared by adding 150 mg of GO to 25 mL of deionized water and ultrasonically dispersed for 3 hours. Subsequently, 300 mg of L-ascorbic acid was added as reducing agent, and the mixture was ultrasonicated for 30 min to make it uniformly dispersed, and then it was transferred to a hydrothermal autoclave reactor and kept at constant temperature of 90 °C for 12 h. After the reactor was cooled to room temperature the 3D graphene hydrogel was taken out and then washed with deionized water to remove the residual L-ascorbic acid. Finally, the 3D graphene hydrogel was freeze-dried at −60 °C for 72 hours to obtain 3D-rGO.

2.1.2 Preparation of 3D-rGO/SDBS. A certain concentration of GO suspension was prepared according to the above method, and a mixed solution was prepared by adding SDBS (the mass ratio of GO to SDBS was 1 : 1), followed by ultrasonication for 1 hour to make the mixture well dispersed. Then L-ascorbic acid was added to the mixed solution (the mass ratio of GO and L-ascorbic acid was 1 : 4) and the sonication process was continued for 1 h. Subsequently, the solution was transferred to hydrothermal autoclave reactor and reacted at a constant

temperature of 90 °C for 12 h. The hydrogels taken out were washed and freeze-dried in the same way to obtain 3D-rGO/SDBS.

2.2 Characterization

The microscopic morphology of the materials was observed using a scanning electron microscope (SEM, model SU8010, Hitachi Co., Ltd, Tokyo, Japan) with an accelerating voltage of 20 kV. An X-ray diffractometer (XRD, model D8 Advance, Bruker AXS Inc., Billerica, MA, USA) was used to characterize the crystal structure of the materials using Cu Kα X-rays. The diffraction angle 2θ was analysed over a range of 5° to 90° with an operating voltage of 40 kV and a scanning step of 0.03°. Changes in the chemical composition of graphene-based materials were analysed using a Fourier transform infrared spectrometer (FTIR, model Nicolet IS50, Thermo Fisher Scientific Inc., Waltham, MA, USA) with a scan range of 400 to 4000 cm^{-1}. The structural characterization of the materials was carried out using a Raman spectrometer (model Renishaw in *Via*, Renishaw PLC., Wotton-under-Edge, Gloucestershire, UK) with a laser wavelength of 532 nm and a wave number range of 100 to 3500 cm^{-1}. The nitrogen adsorption and desorption isotherm (77 K) of the 3D-rGO/SDBS material was tested using a surface area and porosity analyser (model TriStar II 3020, Micromeritics Instrument Corp., Norcross, Georgia, USA). The surface area was calculated based on the Brunauer–Emmett–Teller (BET) method. The total pore volume was evaluated based on adsorption branch at a relative pressure of 0.99 and the pore size distribution was calculated using the Barrett–Joyner–Halenda (BJH) method.

2.3 Methane hydrate formation

2.3.1 Apparatus. The methane hydrate formation device used in this study is shown in Fig. 1, which mainly consists of gas supply system including gas cylinder and buffer tank, reaction system including a transparent high-pressure reaction kettle and stirring device, temperature and pressure control system, and data acquisition system. The methane hydrate formation experiments were carried out in the transparent high-pressure reaction kettle with an effective volume of 73 mL and a pressure range of 0–20 MPa. The reaction kettle was equipped with an O-type magnetic stirrer, which was driven by an electric motor to pull it with up-and-down reciprocating motions to mix the reactants in the kettle. The methane gas is supplied from a gas cylinder. 126 mL effective volume stainless steel buffer tank (pressure range 0–50 MPa) is used to cool the methane gas in advance. The temperature of the buffer tank and the reaction kettle was controlled by a high-low temperature test chamber. In order to monitor the pressure variation of the system, the pressure sensor (uncertainty = ± 0.1%, pressure range 0–20 MPa) was installed on the buffer tank and the reaction kettle respectively. The data acquisition system recorded pressure data every minute.

2.3.2 Procedure. Five systems of pure water, SDBS solution, GO-water, 3D-rGO-water, and 3D-rGO/SDBS-water were constructed and used for methane hydrate formation, in which the type of promoter added to the three systems, namely, GO-water, 3D-rGO-water, and 3D-rGO/SDBS-water, was graphene material. In order to maintain consistency of the comparative studies, all promoters were added at a concentration of 600 ppm.

The reaction kettle was first washed with deionized water and then filled it with 10 mL of the configured solution after the kettle was dry. The kettle was then fixed in the high-low temperature test chamber and sealed tightly. The buffer tank and kettle were evacuated, then filled with methane and evacuated again to remove the air. Subsequently, methane at a pressure higher than the experimental pressure (about 10 MPa) was injected into the buffer tank. The temperature of the high-low temperature test chamber was set to the experimental temperature of 275.15 K to achieve cooling of the gas in the buffer tank and the solution in the kettle. When the pressure fluctuation in the buffer tank was less than 5 kPa for at least 30 min, methane was injected from the buffer tank into the reaction kettle to the required pressure for the experiment, and then the inlet valve of the kettle was closed. Then the magnetic stirring (rotating speed of 300 rpm) was immediately turned on. Finally, methane hydrate was formed in the reactor kettle.

In addition, the methane hydrate formation kinetics in the 3D-rGO/SDBS-water system at concentrations of 200, 400, 600,

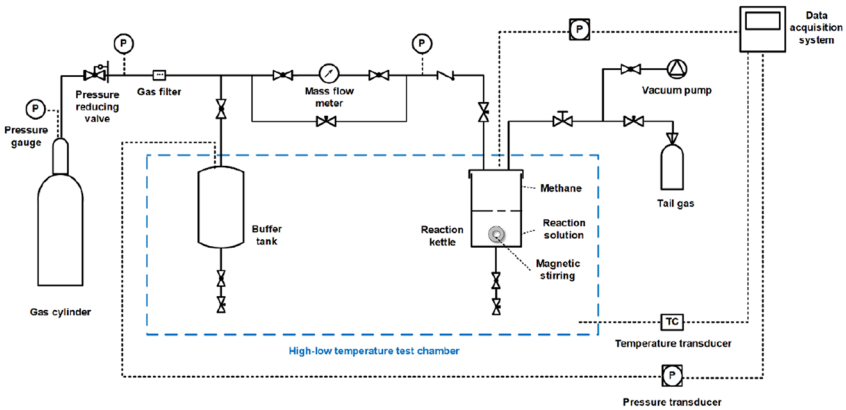

Fig. 1 Schematic diagram of the experimental apparatus.

and 800 ppm were tested. The operating procedures were consistent with the five systems described above.

2.3.3 Data Processing. The total number of moles of methane ($n_{a,t}$) injected from the buffer tank into the reaction kettle at time t during hydrate formation is calculated by eqn (1):

$$n_{a,t} = \frac{P_{a,0}V_a}{Z_{a,0}RT} - \frac{P_{a,t}V_a}{Z_{a,t}RT} \quad (1)$$

where P_a and V_a are the pressure and volume of the buffer tank. T is the experimental temperature. The subscript 0 denotes the time of methane injection from the buffer tank into the reaction kettle. R is the universal gas constant. Z is the compressibility factor which is calculated by the Peng–Robinson equation of state.[31]

The number of moles of gas-phase methane ($n_{g,t}$) in the reaction kettle at time t is calculated by eqn (2), where the dissolved consumed methane is not taken into account due to the too small amount dissolved.[32]

$$n_{g,t} = \frac{P_{g,t}V_{g,t}}{Z_{g,t}RT} \quad (2)$$

where $P_{g,t}$ and $V_{g,t}$ are the pressure and gas phase volume of the reaction kettle. $V_{g,t}$ is calculated by eqn (3):

$$V_{g,t} = V_b - V_l(1 - x_t) - 1.25V_l x_t \quad (3)$$

where V_b and V_l are the volumes of the reaction kettle and the solution in the kettle, respectively, and x_t is the water-to-hydrate conversion ratio. The volume expansion coefficient of methane hydrate is taken as 1.25.[33]

The number of moles of captured gas (n_h) in the hydrate at time t is calculated from eqn (4):

$$n_{h,t} = \frac{m_l x_t}{18 \times 5.94} \quad (4)$$

where, m_l is the mass of the solution, the molar mass of the solution is approximated to the molar mass of water as the content of accelerator in the solution is only at ppm-level, which is taken as 18 in this study. The hydration number of methane hydrate is taken as 6.[34]

The mass balance of methane in the reaction kettle can be expressed as eqn (5) below:

$$n_{a,t} = n_{g,t} + n_{h,t} \quad (5)$$

Combining eqn (1)–(5) gives the water-to-hydrate conversion ratio (x_t):

$$x_t = \left[n_{a,t} - \frac{P_{g,t}(V_b - V_l)}{Z_{g,t}RT}\right] \Big/ \left(\frac{m_l}{108} - \frac{0.25P_{g,t}V_l}{Z_{g,t}RT}\right) \quad (6)$$

The gas storage capacity (C_s, in v/v_w) of the system at moment t is defined as the ratio of the volume of captured gas to solution, and is calculated by eqn (7):

$$C_s = 22.4n_h/V_l \quad (7)$$

Experiments with pure, single-phase methane gas will only form sI hydrates, both in the pure water system and in the system with the addition of different types of kinetic promoters.[35] The sI methane hydrate can be stable over a wide range of pressures and temperatures, and kinetic promoters do not affect the structure.[36,37] In sI methane hydrate, the theoretical ratio of water to gas in hydrate is 5.75 mol mol^{-1} with all cavities filled with gas molecules.[38] That is, in these experiments one volume of water can theoretically encapsulate 216 volumes (STP) of methane gas.[39] The methane storage capacity of each system is calculated and compared with the theoretical value.

3 Results and discussion

3.1 Characterization of GO, 3D-rGO and 3D-rGO/SDBS

SEM images show that GO presents 2D lamellar structure with ripple-like folds and wide and large surface (Fig. 2a). In contrast, the interior of 3D-rGO presents interconnected 3D porous structure (Fig. 2b), which is formed by self-assembly of GO sheets, so that the 3D-rGO surface still retains the folds of GO, resulting in a larger surface. The 3D porous structure inside the composite 3D-rGO/SDBS is well maintained (Fig. 2c), indicating that the π-like stacking of SDBS on the graphene surface does not disrupt the 3D structural features of 3D-rGO/SDBS.

The XRD spectra of GO, 3D-rGO and 3D-rGO/SDBS are shown in Fig. 3a. It can be seen that the peak at 2θ of 8.78° is the (001) characteristic diffraction peak of GO,[40] and the layer spacing of GO is calculated to be 1.005 nm according to Bragg's equation.[41] The reason for the relatively large layer spacing of GO is the grafting of many oxygen-containing groups on its surface. When GO is chemically reduced, the diffraction peak located at 8.78° disappears utterly, and a broad and weak (002) diffraction peak of 3D-rGO appears at 2θ of 25.41°,[42] and the lamellar spacing is reduced to 0.350 nm. This is attributed to the fact that the chemical reduction process efficiently eliminates the oxygen-containing groups grafted on the surface of GO, and its product, reduced graphene oxide (rGO) flakes, self-assemble to form 3D structure. This process reduces phonon scattering due to oxygen-containing groups and excessive individual dispersed interfaces, enhances phonon transport, and thus improves the thermal conductivity of 3D graphene materials.[43] The XRD spectra of 3D-rGO and 3D-rGO/SDBS show similar shapes, which change only by a shift of the broad diffraction peak from 25.41° to a lower angle of 24.21°, corresponding to an increase in the interlayer spacing from 0.350 nm to 0.367 nm. This result indicates that the reduced rGO surface was re-grafted with new groups, resulting in a slight increase in the lamellar spacing of rGO, which suggests that SDBS was successfully bound to the 3D-rGO surface to form 3D-rGO/SDBS. In addition, SDBS

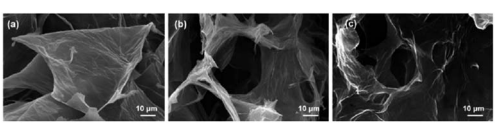

Fig. 2 The SEM images of (a) GO, (b) 3D-rGO and (c) 3D-rGO/SDBS.

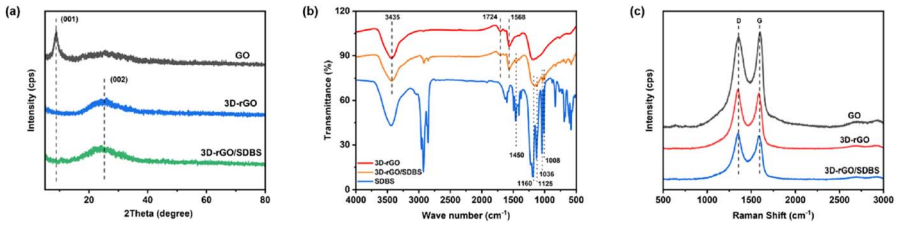

Fig. 3 (a) XRD and (c) Raman spectra of GO, 3D-rGO and 3D-rGO/SDBS; (b) Infrared spectra of 3D-rGO, 3D-rGO/SDBS and SDBS.

grafted on the graphene surface could keep 3D-rGO/SDBS dispersed and stable in solution.

Fig. 3b shows the infrared spectra of 3D-rGO, 3D-rGO/SDBS and SDBS. Comparing 3D-rGO, four new characteristic peaks attributed to the sulfonic acid group of SDBS appeared in 3D-rGO/SDBS at 1160, 1125, 1036, and 1008 cm^{-1}; in addition, a new characteristic peak also appeared at 1450 cm^{-1}, which was the effect of C=C bond of the benzene ring of SDBS and the C=C bond of 3D-rGO. These test results further indicate that SDBS and 3D-rGO have been successfully combined. For 3D-rGO and 3D-rGO/SDBS, the peak at 3435 cm^{-1} is attributed to the O–H stretching vibration of the hydroxyl group, the peak near 1724 cm^{-1} is attributed to the C=O stretching vibration of the carboxyl group, and the peak near 1568 cm^{-1} is attributed to the C–H stretching vibration. The intensities of the above three peaks in both 3D-rGO and 3D-rGO/SDBS spectra are weakened compared with GO (Fig. S1†), indicating that only few oxygen-containing groups remain on the surface of GO after chemical reduction, and the reduction process is relatively thorough.

Fig. 3c shows the Raman spectra of GO, 3D-rGO and 3D-rGO/SDBS, the 1350 cm^{-1} characteristic peak corresponds to the disordered vibration peak (D peak) of graphene, and the 1590 cm^{-1} characteristic peak corresponds to vibration of sp^2 hybridization carbon atoms on the hexagonal lattice of graphene peak (G peak). The larger intensity ratio (I_D/I_G) of the D and G peaks indicates that the disorder of the material is higher.[44] As can be seen from the figure, the I_D/I_G of 3D-rGO and 3D-rGO/SDBS is higher than that of GO, which indicates that the disorder of graphene increases after chemical reduction. The reduction process causes 3D-rGO to produce more planar defects, which can be used as nucleation sites for hydrates.[45,46]

The nitrogen adsorption and desorption isotherm and pore size distribution of 3D-rGO are shown in Fig. 4. It can be seen that 3D-rGO reveals typical type IV isotherms with H3-type hysteresis loops, which indicates that the sample is rich in mesopores, and the corresponding pore size distributions confirm this. Most importantly, the 3D-rGO formed by chemical reduction and self-assembly of 2D GO sheets has huge specific surface area of 1443 $m^2\ g^{-1}$ and a pore volume of 2.36 $cm^3\ g^{-1}$.

3.2 Methane hydrate formation

Fig. 5a shows the variation of gas pressure during methane hydrate formation, which was used to investigate the dependence of methane hydrate formation on the type of promoter. The experimental temperature was 275.15 K, the initial pressure was 6 MPa, and the stirring speed was 300 rpm. The promoter types included SDBS, GO, 3D-rGO and 3D-rGO/SDBS, and pure water was used as a control group. Taking pure water as an example, it can be seen that the typical pressure changes during the formation of methane hydrate are as follows: the pressure is relatively stable at first (induction stage), followed by a rapid decrease in pressure (hydrate formation stage in large quantities), and then the pressure returns to be stable again (end of hydrate formation). The trend of the pressure change curves in each system is similar, but the specific behaviour at each stage is quite different.

The induction time, defined as the time required from the initial equilibrium state to hydrate nucleation, is a key parameter to quantify the nucleation process of methane hydrates.[47,48] It can provide information about the kinetics of hydrate nucleation and growth.[49] Fig. 5b shows the induction time of methane hydrate formation in the presence of different types of promoters. The results showed that the addition of GO, 3D-rGO and 3D-rGO/SDBS all significantly shortened the induction time

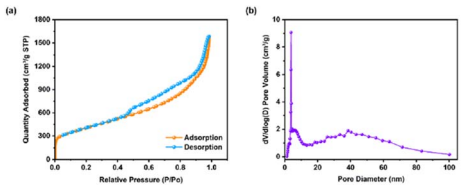

Fig. 4 (a) 77 K nitrogen adsorption and desorption isotherms and (b) pore size distribution of 3D-rGO.

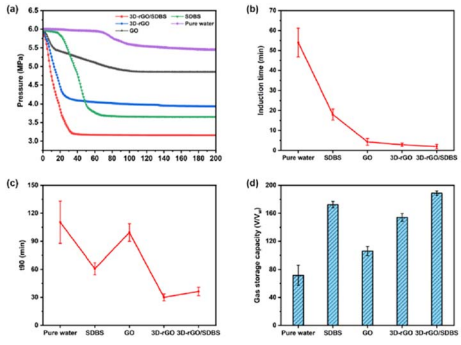

Fig. 5 (a) Pressure changes, (b) induction time, (c) t_{90} and (d) gas storage capacity of methane hydrate formation in the systems of pure water, SDBS, GO, 3D-rGO and 3D-rGO/SDBS at 275.15 K and 6 MPa.

of hydrate formation. Among them, the induction time of hydrate formation in the 3D-rGO/SDBS system was the shortest at 1.9 min, which was 96.5% shorter than that of the pure water system (53.9 min) and 89.3% shorter than that of the SDBS system (17.7 min) on average. The larger specific surface area of graphene can provide more nucleation sites for hydrates at the initial stage, which has been shown to be effective in promoting the non-homogeneous nucleation of hydrates. In addition to its huge specific surface area, the interconnected 3D porous structure of 3D-rGO/SDBS upscales the 2D material into free-standing 3D space with better thermal conductivity, which is capable of releasing the heat generated from hydrate formation in time and accelerating the hydrate nucleation kinetics.

t_{90} is the time taken for 90% completion of hydrate formation and is important for measuring the formation cycle of hydrate.[50] Fig. 5c shows the effect of the addition of different types of promoters on t_{90}. While the t_{90} of the pure water system was about 111 min, the presence of 3D-rGO and 3D-rGO/SDBS significantly reduced the t_{90} to less than 35 min, shortening the formation cycle of hydrate by about 68.5%. Previous studies have shown that SDBS is able to reduce the surface tension of the solution without forming a hydrate film covering the entire methane–water interface, which enhances the mass transfer from the gas phase to the liquid phase, and the formation cycle of hydrate is thus shortened.[51] Furthermore, according to Kim *et al.* excessive oxygen-containing groups on the surface of GO produce strong interactions with the surrounding water molecules and reduce the water activity, thus inhibiting the rapid formation of gas hydrates.[52] In this study, we compare the t_{90} of 3D-rGO/SDBS, 3D-rGO, SDBS, and GO and find that methane is trapped at a faster rate in the 3D-rGO/SDBS and 3D-rGO systems, and that the substantial reduction in the formation cycle of hydrate correlates with the 3D graphene structure. On the one hand, most of the oxygen-containing groups on the surface of GO are eliminated due to the chemical reduction process, which largely attenuates the effect of oxygen-containing groups on water activity. On the other hand, 3D-rGO formed by self-assembly of rGO sheets has 3D porous structure, which can adsorb nonpolar methane molecules both on its surface and within its pore size, significantly increasing the solubility of methane in solution. In addition, the rate of gas consumption is restricted by the dispersion rate of gas in the bulk solution.[53] The 3D-rGO dispersed in solution promotes the mass transfer of methane and the rate of hydrate formation is subsequently accelerated.

Fig. 5d shows the final gas storage capacity of each system in the presence of different types of promoters. It can be seen that the gas storage capacity of pure water is only 71 v/v_w, which is 33% of the theoretical maximum storage capacity, and the addition of 3D-rGO/SDBS increases this result to about 188 v/v_w, which is 87% of the theoretical value. The higher gas storage capacity of 3D-rGO/SDBS compared to that of SDBS suggests that the combination of 3D-rGO and SDBS may have synergistically promoted methane hydrate formation. And the excellent specific surface area of 3D-rGO/SDBS can bind more SDBS. In addition to the adsorption of methane by the 3D structure itself, the numerous $-SO_3^-$ groups of SDBS on the surface of 3D-rGO/SDBS are able to bind more water molecules, and methane and water are aggregated in the vicinity of 3D-rGO/SDBS, and the chances of contacting the two are significantly increased, which is conducive to the sustained formation of methane hydrates.

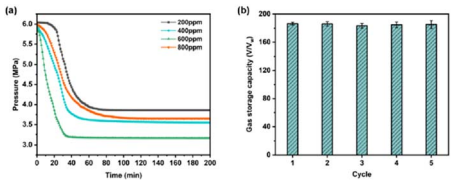

Fig. 6 (a) Pressure changes of methane hydrate formation with 3D-rGO/SDBS of different additions; (b) gas storage capacity of methane hydrate formation for 5 cycles with 3D-rGO/SDBS addition of 600 ppm at 275.15 K and 6 MPa.

Fig. 6a shows the effects of different additions of 3D-rGO/SDBS on the methane hydrate formation process. The corresponding induction time, t_{90} and gas storage capacity are shown in Fig. S2–S4.† Among all the systems, the induction time and formation cycle of hydrate are shortest and the gas storage capacity is highest when the addition amount of 3D-rGO/SDBS is 600 ppm. This may be due to the strongest synergistic effect on methane hydrate formation by the combination of 3D-rGO and SDBS at 600 ppm. When the addition amount of 3D-rGO/SDBS continues to increase to 800 ppm, the formation cycle of hydrate becomes longer and the gas storage capacity decreases. The gas storage capacity of 3D-rGO/SDBS (600 ppm addition) after five methane hydrate formation-dissociation cycles is shown in Fig. 6b. The gas storage capacity was stabilized at around 185 v/v_w (86% of the theoretical value) for all five cycling experiments, which indicates that 3D-rGO/SDBS has excellent cycling stability performance and can be recycled and reused many times.

3.3 Analysis of promoting mechanisms

Fig. 7 shows the schematic diagram of the methane hydrate formation process in pure water, where hydrate nucleation usually occurs at the gas–liquid interface due to a higher initial methane concentration than that of the bulk phase. Nucleation of crystals in the liquid phase is characterized by the existence of the crystal-liquid interfacial energy barrier, and a sufficiently large number of molecules must be aggregated to form nuclei larger than critical size, so a long induction time is required for hydrate formation in pure water.[54] The growth of hydrate uses the gas–liquid interface as the reaction surface and gradually

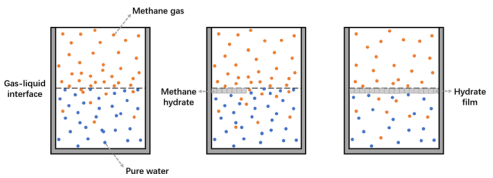

Fig. 7 Schematic of methane hydrate formation in pure water.

forms a hydrate film covering the entire interface. This hydrate film separates the gas phase from the liquid phase, which severely weakens the gas–liquid mass transfer, and the rate of hydrate formation slows down or even stops.

As shown in Fig. 8, the addition of SDBS can improve the above situation. The hydrophilic head of the SDBS molecule attracts water molecules through polar interactions, which reduces the surface tension of the solution. Meanwhile, the non-polar hydrocarbon chains of SDBS can adsorb methane gas, increasing the amount and rate of methane dissolution in solution. Based on this, the chance of hydrate film formation at the gas–liquid interface in the SDBS system is significantly reduced, and the limitation of the hydrate film on the gas–liquid mass transfer will disappear, resulting in the shortening of the induction time and accelerating of the formation rate of hydrate.

As shown in Fig. 9, 3D-rGO/SDBS combines the advantages of 3D-rGO and SDBS for solidified gas efficient storage. During the initial induction phase, on the one hand, the solid surface can provide the supercritical size required for hydrate nucleation and reduce the effect from the interfacial energy. 3D graphene has 3D space and superior specific surface area, so 3D-rGO/SDBS in solution can form many non-homogeneous nucleation centers and use heterogeneous effect to avoid the formation of hydrate film. On the other hand, the chemical reduction process efficiently eliminates the oxygen-containing groups grafted on the surface of GO, which can reduce the in-plane phonon scattering and enhance phonon transport.[55–57] In addition, the self-assembly of individual dispersed 2D graphene to form 3D continuous network structure can effectively decrease the amount of interfaces, which in turn decreases the boundary interface phonon scattering and the interfacial thermal resistance, and further improves the thermal conductivity of 3D-rGO/SDBS.[58–60] As a result, the heat generated from hydrate generation can be released in time for rapid nucleation. In the hydrate formation stage in large quantities, the 3D space of 3D-rGO/SDBS can adsorb more methane molecules, which increases the dissolution of methane in solution. And the dispersion of 3D-rGO/SDBS in solution also accelerates the mass transfer process of methane in the liquid phase. Compared with SDBS solution, 3D-rGO/SDBS surface binds more SDBS molecules, which can adsorb more water molecules to interact with methane, thus shortening the formation cycle of hydrate, increasing the final gas storage capacity, and breaking the kinetic limitation of the formation process of artificial methane hydrate.

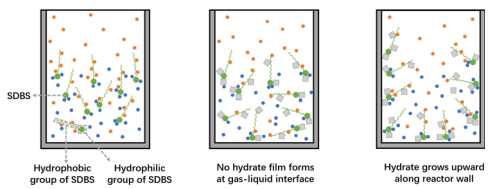

Fig. 8 Schematic diagram of methane hydrate formation after addition of SDBS.

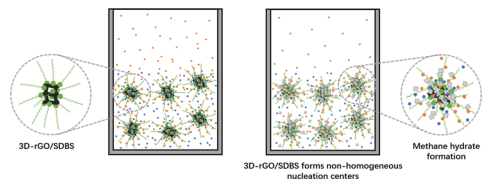

Fig. 9 Schematic diagram of methane hydrate formation after addition of 3D-rGO/SDBS.

4 Conclusions

In this study, the effects of the presence of SDBS, GO, 3D-rGO and 3D-rGO/SDBS on the induction time, formation cycle, and final gas storage capacity during the formation of methane hydrates were investigated. The experimental results show that 3D-rGO/SDBS combines the advantages of 3D-rGO and SDBS, and can promote methane hydrate formation in terms of both structure and surface properties. The maximum methane storage capacity of 188 v/v_w is obtained with 600 ppm of 3D-rGO/SDBS in water, reaching 87% of the theoretical maximum storage capacity, which can realize the efficient storage of methane gas. And the addition of 3D-rGO/SDBS also significantly shortens the induction time and accelerates the formation rate of methane hydrate with excellent kinetic promotion. In addition, 3D-rGO/SDBS shows excellent cyclic stability performance during five methane hydrate formation–dissociation processes, and has the potential to be used as an environmentally-friendly, fast, and efficient promoter to support SNG technology.

Conflicts of interest

There are no conflicts of interest to declare.

References

1 C. A. Koh, A. K. Sum and E. D. Sloan, State of the art: Natural gas hydrates as a natural resource, *J. Nat. Gas Sci. Eng.*, 2012, **8**, 132–138.
2 E. D. Sloan and C. A. Koh, *Clathrate Hydrates of Natural Gases*, CRC press, 2007.
3 Y. F. Makogon, S. A. Holditch and T. Y. Makogon, Natural gas-hydrates—A potential energy source for the 21st Century, *J. Pet. Sci. Eng.*, 2007, **56**, 14–31.
4 H. P. Veluswamy, A. Kumar, R. Kumar and P. Linga, An innovative approach to enhance methane hydrate formation kinetics with leucine for energy storage application, *Appl. Energy*, 2017, **188**, 190–199.
5 K. B. Yu and A. O. Yazaydin, Does Confinement Enable Methane Hydrate Growth at Low Pressures? Insights from Molecular Dynamics Simulations, *J. Phys. Chem. C*, 2015, **124**, 11015–11022.
6 S. Takeya, A. Hori, T. Hondoh and T. Uchida, Freezing-memory Effect of Water on Nucleation of CO_2 Hydrate Crystals, *J. Phys. Chem. B*, 2000, **104**, 4164–4168.

7 M. E. Casco, J. Silvestre-Albero, A. J. Ramírez-Cuesta, F. Rey, J. L. Jordá, A. Bansode, A. Urakawa, I. Peral, M. Martínez-Escandell, K. Kaneko and F. Rodríguez-Reinoso, Methane hydrate formation in confined nanospace can surpass nature, *Nat. Commun.*, 2015, **6**, 6432.

8 K. U. Heeschen, J. M. Schicks and G. Oeltzschner, The promoting effect of natural sand on methane hydrate formation: Grain sizes and mineral composition, *Fuel*, 2016, **181**, 139–147.

9 G. C. Fitzgerald, M. J. Castaldi and J. M. Schicks, Methane Hydrate Formation and Thermal Based Dissociation Behavior in Silica Glass Bead Porous Media, *Ind. Eng. Chem. Res.*, 2014, **53**, 6840–6854.

10 Y. Zhang, L. Zhang, C. Y. Zhu, L. X. Xu, X. S. Li and Z. Y. Chen, Formation Behaviors of Methane Hydrate in Partially Water-Saturated Porous Media with Different Particle Sizes, *Energy Fuels*, 2021, **35**, 19399–19409.

11 B. H. Shi, L. Yang, S. S. Fan and X. Lou, An investigation on repeated methane hydrates formation in porous hydrogel particles, *Fuel*, 2017, **194**, 395–405.

12 S. Denning, A. A. A. Majid, J. M. Lucero, J. M. Crawford, M. A. Carreon and C. A. Koh, Metal–Organic Framework HKUST-1 Promotes Methane Hydrate Formation for Improved Gas Storage Capacity, *ACS Appl. Mater. Interfaces*, 2020, **12**, 53510–53518.

13 H. Q. Liu, Y. C. Song, C. R. Shi, J. F. Zhao and Z. Ling, Investigating the synergistic initiating effect on promoting methane hydrate formation via mixed graphene and sodium cholate, *J. Mol. Liq.*, 2022, **349**, 118134.

14 A. McElligott, J. L. Meunier and P. Servio, Effects of nitrogen-doped graphene nanoflakes on methane hydrate formation, *J. Nat. Gas Sci. Eng.*, 2021, **96**, 104336.

15 S. Yan, W. J. Dai, S. L. Wang, Y. C. Rao and S. D. Zhou, Graphene Oxide: An Effective Promoter for CO_2 Hydrate Formation, *Energies*, 2018, **11**, 1756.

16 A. Ghozatloo, M. Hosseini and M. Shariaty-Niassar, Improvement and enhancement of natural gas hydrate formation process by Hummers' graphene, *J. Nat. Gas Sci. Eng.*, 2015, **27**, 1229–1233.

17 M. Hosseini, A. Ghozatloo and M. Shariaty-Niassar, Effect of CVD graphene on hydrate formation of natural gas, *J. Nanostruct. Chem.*, 2015, **5**, 219–226.

18 H. Q. Liu, Y. C. Song, C. R. Shi, J. F. Zhao and Z. Ling, Investigating the synergistic initiating effect on promoting methane hydrate formation via mixed graphene and sodium cholate, *J. Mol. Liq.*, 2021, **349**, 118134.

19 D. Li, M. B. Müller, S. Gilje, R. B. Kaner and G. G. Wallace, Processable aqueous dispersions of graphene nanosheets, *Nat. Nanotechnol.*, 2008, **3**, 101–105.

20 W. Chen and L. Yan, In situ self-assembly of mild chemical reduction graphene for three-dimensional architectures, *Nanoscale*, 2011, **3**, 3132–3137.

21 R. M. Firdaus, N. Berrada, A. Desforges, A. R. Mohamed and B. Vigolo, From 2D Graphene Nanosheets to 3D Graphene-based Macrostructures, *Chem. - Asian J.*, 2020, **15**, 2902–2924.

22 J. H. Han, I. Johnson and M. W. Chen, 3D Continuously Porous Graphene for Energy Applications, *Adv. Mater.*, 2021, **34**, 2108750.

23 F. Wang, F. P. Song, C. Li and M. T. Sun, Promoted methane hydrate formation in $-SO_3^-$-rich hydrogel clathrate, *Fuel*, 2022, **323**, 124398.

24 A. N. Nesterov, A. M. Reshetnikov, A. Y. Manakov, T. V. Rodionova, E. A. Paukshtis, I. P. Asanov, S. P. Bardakhanov and A. I. Bulavchenko, Promotion and inhibition of gas hydrate formation by oxide powders, *J. Mol. Liq.*, 2015, **204**, 118–125.

25 A. McElligott, J. L. Meunier and P. Servio, Effects of nitrogen-doped graphene nanoflakes on methane hydrate formation, *J. Nat. Gas Sci. Eng.*, 2021, **96**, 104336.

26 F. Wang, H. L. Meng, G. Guo, S. J. Luo and R. B. Guo, Methane hydrate formation promoted by $-SO_3^-$-coated graphene oxide nanosheets, *ACS Sustainable Chem. Eng.*, 2018, **5**, 6597–6604.

27 Z. E. Zhang, Z. M. Liu, Z. Pan, F. M. Baena-Moreno and M. R. Soltanian, Effect of porous media and its distribution on methane hydrate formation in the presence of surfactant, *Appl. Energy*, 2020, **261**, 114373.

28 F. Palazzesi, M. Calvaresi and F. Zerbetto, A molecular dynamics investigation of structure and dynamics of SDS and SDBS micelles, *Soft Matter*, 2011, **7**, 9148–9156.

29 S. H. Zhou, D. L. Wei, H. Y. Shi, X. Feng, K. W. Xue, F. Zhang and W. B. Song, Sodium dodecyl benzene sulfonate functionalized graphene for confined electrochemical growth of metal/oxide nanocomposites for sensing application, *Talanta*, 2013, **107**, 349–355.

30 H. Y. Sun and X. N. Yang, Molecular simulation of self-assembly structure and interfacial interaction for SDBS adsorption on graphene, *Colloids Surf., A*, 2014, **462**, 82–89.

31 D. Y. Peng and D. B. Robinson, A new two-constant equation of state, *Indian J. Pure Appl. Math.*, 1976, **15**, 59–64.

32 L. K. Wang, G. J. Chen, G. H. Han, X. Q. Guo and T. M. Guo, Experimental study on the solubility of natural gas components in water with or without hydrate inhibitor, *Fluid Phase Equilib.*, 2003, **207**, 143–154.

33 P. Xiao, X. M. Yang, C. Y. Sun, J. L. Cui, N. Li and G. J. Chen, Enhancing methane hydrate formation in bulk water using vertical reciprocating impact, *Chem. Eng. J.*, 2018, **336**, 649–658.

34 V. D. Chari, P. S. R. Prasad and S. R. Murthy, Structural stability of methane hydrates in porous medium: Raman spectroscopic study, *Spectrochim. Acta, Part A*, 2014, **120**, 636–641.

35 C. A. Koh, Towards a fundamental understanding of natural gas hydrates, *Chem. Soc. Rev.*, 2002, **31**, 157–167.

36 Y. F. Makogon, Natural gas hydrates – A promising source of energy, *J. Nat. Gas Sci. Eng.*, 2010, **2**, 49–59.

37 A. Kumar, G. Bhattacharjee, B. D. Kulkarni and R. Kumar, Role of Surfactants in Promoting Gas Hydrate Formation, *Ind. Eng. Chem. Res.*, 2015, **54**, 12217–12232.

38 H. Ganji, M. Manteghian, K. S. Zadeh, M. R. Omidkhah and H. R. Mofrad, Effect of different surfactants on methane

hydrate formation rate, stability and storage capacity, *Fuel*, 2007, **86**, 434–441.

39 E. D. Sloan, Fundamental principles and applications of natural gas hydrates, *Nature*, 2003, **426**, 353–359.

40 T. T. Vu, T. C. Hoang, T. H. L. Vu, T. S. Huynh and T. V. La, Template-free fabrication strategies for 3D nanoporous Graphene in desalination applications, *Arabian J. Chem.*, 2021, **14**, 103088.

41 C. G. Pope, X-ray diffraction and the Bragg equation, *J. Chem. Educ.*, 1997, **74**, 129–131.

42 L. Zhang and G. Q. Shi, Preparation of Highly Conductive Graphene Hydrogels for Fabricating Supercapacitors with High Rate Capability, *J. Phys. Chem. C*, 2011, **115**, 17206–17212.

43 S. C. Lin and M. J. Buehler, Thermal transport in monolayer graphene oxide: Atomistic insights into phonon engineering through surface chemistry, *Carbon*, 2014, **77**, 351–359.

44 T. Kuila, S. Bose, A. K. Mishra, P. Khanra, N. H. Kim and J. H. Lee, Chemical functionalization of graphene and its applications, *Prog. Mater. Sci.*, 2012, **57**, 1061–1105.

45 Y. Y. Peng, Y. M. Liu, J. K. Chang, C. H. Wu, M. D. Ger, N. W. Pu and C. L. Chang, A facile approach to produce holey graphene and its application in supercapacitors, *Carbon*, 2015, **81**, 347–356.

46 H. Q. Liu, Y. C. Song, C. R. Shi, J. F. Zhao and Z. Ling, Investigating the synergistic initiating effect on promoting methane hydrate formation via mixed graphene and sodium cholate, *J. Mol. Liq.*, 2022, **349**, 118134.

47 D. Kashchiev and A. Firoozabadi, Induction time in crystallization of gas hydrates, *J. Cryst. Growth*, 2003, **250**, 499–515.

48 S. R. Wang, M. J. Yang, W. G. Liu, J. F. Zhao and Y. C. Song, Investigation on the induction time of methane hydrate formation in porous media under quiescent conditions, *J. Pet. Sci. Eng.*, 2016, **145**, 565–572.

49 S. Abedi-Farizhendi, M. Iranshahi, A. Mohammadi, M. Manteghian and A. H. Mohammadi, Kinetic study of methane hydrate formation in the presence of carbon nanostructures, *Pet. Sci.*, 2019, **16**, 657–668.

50 C. R. Shi, F. Y. Chai, M. J. Yang, Y. C. Song, F. Q. Wang, H. Zhou and Z. Ling, Enhance methane hydrate formation using fungus confining sodium dodecyl sulfate solutions for methane storage, *J. Mol. Liq.*, 2021, **333**, 116020.

51 O. Nashed, B. Partoon, B. Lal, K. M. Sabil and A. M. Shariff, Review the impact of nanoparticles on the thermodynamics and kinetics of gas hydrate formation, *J. Nat. Gas Sci. Eng.*, 2018, **55**, 452–465.

52 D. Kim, D. W. Kim, H. K. Lim, J. Jeon, H. Kim, H. T. Jung and H. Lee, Inhibited phase behavior of gas hydrates in graphene oxide: influences of surface and geometric constraints, *Phys. Chem. Chem. Phys.*, 2014, **16**, 22717–22722.

53 Y. S. Yu, C. G. Xu and X. S. Li, Evaluation of CO_2 hydrate formation from mixture of graphite nanoparticle and sodium dodecyl benzene sulfonate, *J. Ind. Eng. Chem.*, 2018, **59**, 64–69.

54 S. Takeya, A. Hori, T. Hondoh and T. Uchida, Freezing-memory Effect of Water on Nucleation of CO_2 Hydrate Crystals, *J. Phys. Chem. B*, 2000, **27**, 4164–4168.

55 J. J. Chen and L. K. Li, Effect of oxidation degree on the thermal properties of graphene oxide, *J. Mater. Res. Technol.*, 2020, **9**, 13740–13748.

56 H. F. Song and F. Y. Kang, Recent Progress on Thermal Conduction of Graphene, *Acta Phys.-Chim. Sin.*, 2022, **38**, 2101013.

57 S. F. Pei and H. M. Cheng, The reduction of graphene oxide, *Carbon*, 2012, **50**, 3210–3228.

58 Z. W. Chen, X. Y. Zhang and Y. Z. Pei, Manipulation of Phonon Transport in Thermoelectrics, *Adv. Mater.*, 2018, **30**, 1705617.

59 W. Y. Zhang, Q. Q. Kong, Z. C. Tao, J. C. Wei, L. J. Xie, X. Y. Cui and C. M. Chen, 3D Thermally Cross-Linked Graphene Aerogel-Enhanced Silicone Rubber Elastomer as Thermal Interface Material, *Adv. Mater. Interfaces*, 2019, **6**, 1900147.

60 M. Loeblein, S. H. Tsang, M. Pawlik, E. J. R. Phua, H. Yong, X. W. Zhang, C. L. Gan and E. H. T. Teo, High-Density 3D-Boron Nitride and 3D-Graphene for High-Performance Nano-Thermal Interface Material, *ACS Nano*, 2017, **11**, 2033–2044.